ACS APPLIED NANO MATERIALS
Cite This: ACS Appl. Nano Mater. XXXX, XXX, XXX−XXX
Letter
www.acsanm.org

Nanoimaging of Organic Charge Retention Effects: Implications for Nonvolatile Memory, Neuromorphic Computing, and High Dielectric Breakdown Devices

Yingjie Zhang,[*,§,†,‡] Jun Kang,[§] Olivier Pluchery,[*,∥] Louis Caillard,[∥,⊥] Yves J. Chabal,[⊥] Lin-Wang Wang,[§] Javier Fernandez Sanz,[▽] and Miquel Salmeron[*,§,#]

[†]Department of Materials Science and Engineering, University of Illinois, Urbana, Illinois 61801, United States
[‡]Frederick Seitz Materials Research Laboratory, University of Illinois, Urbana, Illinois 61801, United States
[§]Materials Sciences Division, Lawrence Berkeley National Laboratory, Berkeley, California 94720, United States
[∥]Sorbonne Université, UPMC Univ Paris 06, CNRS-UMR 7588, Institut des NanoSciences de Paris, F-75005 Paris, France
[⊥]Laboratory for Surface and Nanostructure Modification, Department of Materials Science and Engineering, University of Texas at Dallas, 800 West Campbell Road, Dallas, Texas 75080, United States
[#]Department of Materials Science and Engineering, University of California, Berkeley, California 94720, United States
[▽]Department Physical Chemistry, Universidad de Sevilla, 41012 Seville, Spain

Supporting Information

ABSTRACT: While a large variety of organic and molecular materials have been found to exhibit charge memory effects, the underlying mechanism is not well-understood, which hinders rational device design. Here, we study the charge retention mechanism of a nanoscale memory system, an organic monolayer on a silicon substrate, with Au nanoparticles on top serving as the electrical contact. Combining scanning probe imaging/manipulation and density functional simulations, we observe stable charge retention effects in the system and attributed it to polaron effects at the amine functional groups. Our findings can pave the way for applications in nonvolatile memory, neuromorphic computing, and high dielectric breakdown devices.

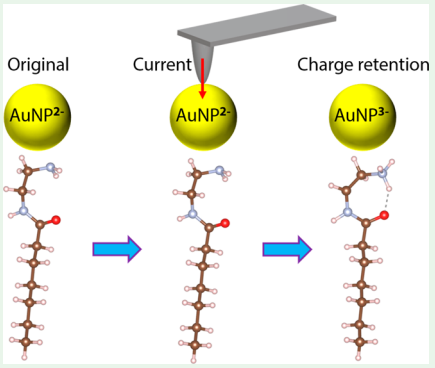

KEYWORDS: *organic monolayer, nanoparticle, charge retention, polaron, Kelvin probe force microscopy, density functional theory, nonvolatile memory*

Organic and molecular materials have been widely explored for large-area electronics applications, such as wearable electronics, solar cells, and display devices.[1−4] A key difference of such organic systems from inorganic structures is the structural flexibility. On one hand, this has been utilized to fabricate flexible and wearable devices, where the electronic functionalities are not affected by mechanical bending and stretching.[1,2] On the other hand, in certain organic materials, the structural reconfiguration is strongly coupled to the electronic states, which can offer new electronic functionality.[5−7] Remarkably, such strong coupling, or polaronic effect, can occur in the size scale as small as a single layer of molecules. Previously, it has been shown that the conformation, charge, or spin states of certain organic monolayers or single molecules can have two or multiple stable configurations that can be switched in the presence of external stimuli such as light or electric current.[6−12] This effect is appealing for a variety of applications ranging from nonvolatile memory, neuromorphic computing, and high dielectric breakdown devices.[13−15] However, so far the mechanism behind the charge state−conformation coupling is not well-understood, which hinders rational material and device design.

Here, we report a combined experimental and computational study of a model molecular memory system. To facilitate charge state imaging and mechanistic understanding of the memory effect, we prepared a grafted organic monolayer (GOM) on a silicon substrate and deposited gold nanoparticles on top as nondestructive electrical contacts to the GOM.[16] We use a scanning probe tip to contact the nanoparticles (NPs) and inject charges into the GOM, and to image the surface potential of the NP. The measured potential reflects the charge state of the GOM underneath the NP.[17−19] We observe a series of charge states at room temperature, which remain stable over a long time (at least 10

Received: June 22, 2019
Accepted: July 24, 2019
Published: July 24, 2019

DOI: 10.1021/acsanm.9b01182
ACS Appl. Nano Mater. XXXX, XXX, XXX−XXX

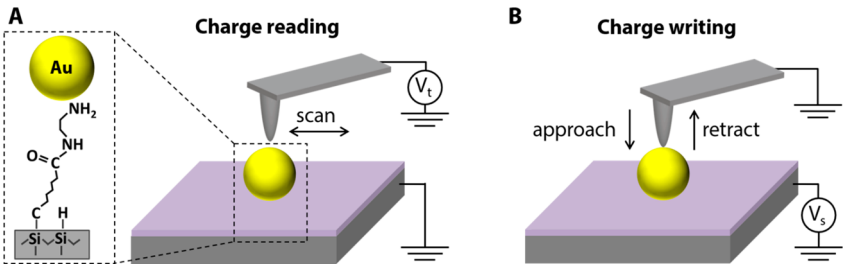

Figure 1. Schematic of the device and measurement setup. (A) Left: molecular structure of the hybrid tunnel junction consisting of silicon/grafted organic monolayer (GOM)/Au nanoparticle (NP). Right: charge state imaging by Kelvin probe force microscopy (KPFM). (B) Charge state manipulation by applying an electric bias (to the sample) while the tip is in contact with the Au NP. V_t: tip bias. V_s: sample bias.

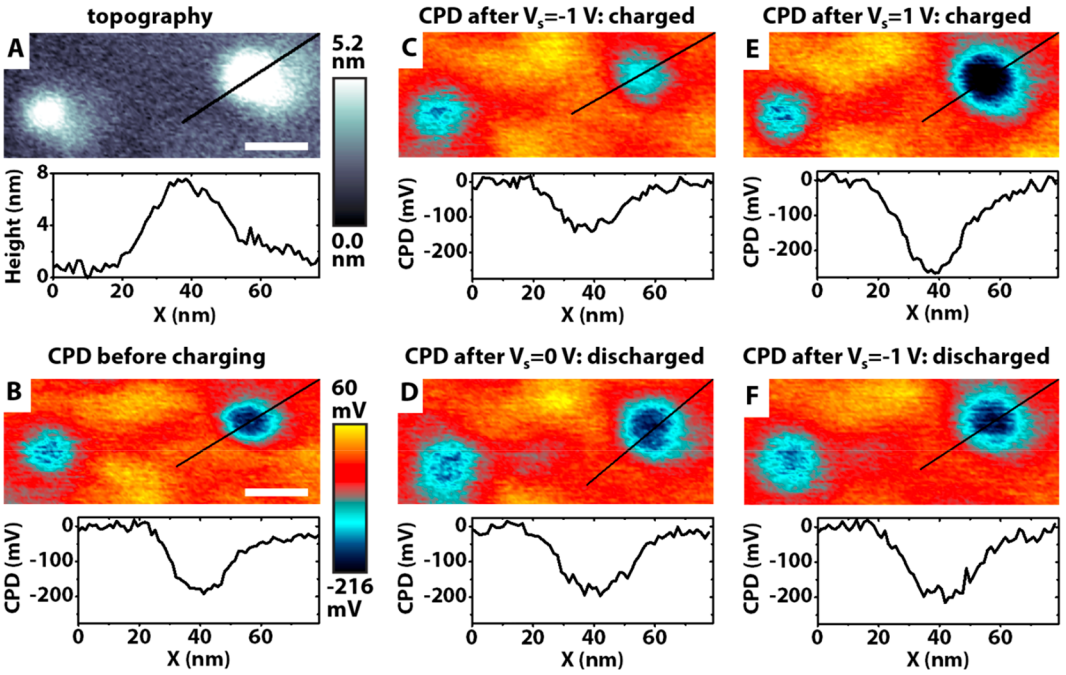

Figure 2. Charge state manipulation of the am-hybrid system. (A) Topographic image of two NPs. The one on the right (with a height of ~7 nm) was approached by the tip to manipulate the charge state, while the one on the left was not contacted during the whole process. (B) Original CPD image of the two NPs on GOM/Si substrate before tip contact. (C) After tip−NP contact with −1 V sample bias, the tip was lifted to image the CPD of the NPs with the substrate grounded. (D−F) Similar to part C, the CPDs of the NPs were imaged after tip−sample contact with different sample bias applied, as labeled. Scale bar: 30 nm. All the images were taken at the same area and have the same size scale. The CPD color scale in parts C−F is the same as that in part B.

h). We did not monitor the charge state of individual NPs for more than 10 h, due to the significant thermal drift of our AFM over such long time periods. We examine the role of molecular distortion on charge stabilization through control experiments, density functional theory calculations, and electrostatic modeling and discuss the implications on memory and computing device applications.

A schematic of the sample and measurement setup is shown in Figure 1. An insulating monolayer film of organic molecules ($-(CH_2)_6-CO-NH-(CH_2)_2-NH_2$) was grafted directly on oxide-free, n-doped silicon (phosphorus doped, 2×10^{18} cm^{-3}).[20,21] Au nanoparticles were deposited on top of the GOM (Figure 1A). The thickness of the GOM was determined to be 1.3 nm by ellipsometry. Due to the substantial contact potential difference (CPD) between Au and the n-doped Si, electrons accumulate in the Au NPs (via tunneling through the GOM) in equilibrium conditions, accompanied by a positive charge depletion layer in the Si. As we showed previously,[17] the charge state of the NP depends on its radius and can be measured from the change in CPD in the Au NP. This CPD was detected by Kelvin probe force microscopy (KPFM),[22−26] a noncontact scanning probe microscopy technique.

Before manipulating the charge state of the system, we measured the CPD of the Au NPs using KPFM (Figure 1A). Then, we electrically grounded the tip and applied a bias to the sample (V_s). The tip was then approached toward the NP at a speed of 1−2 nm/s, allowed to contact the NP for a few seconds (typically 1−5 s) with a load <20 nN, and retracted at the same speed (Figure 1B). After the tip and NP separated, we grounded the sample and acquired KPFM images again (Figure 1A) to determine any change in the charge state. We performed additional measurements by increasing the compression force during tip−NP contact and found that similar results were obtained with the sample topography remaining intact for loads up to ~50 nN. This ensures that the change in charge state is not induced by mechanical forces between the tip and the sample.

DOI: 10.1021/acsanm.9b01182
ACS Appl. Nano Mater. XXXX, XXX, XXX−XXX

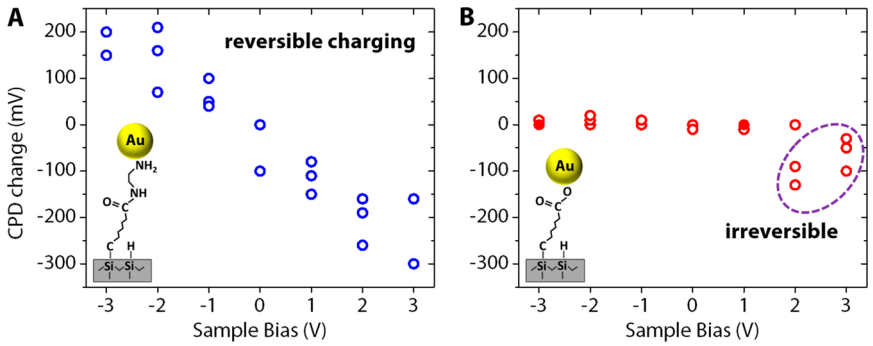

Figure 3. Charge writing at different bias and with different molecules. (A) The Si/GOM/Au NP tunnel junction with aminated molecules exhibits bias-tunable (the sample bias applied during tip−NP contact), reversible charging effects. (B) The junction with nonaminated molecules exhibits no charging effects in the bias range from −3 to 1 V, while small, irreversible CPD changes were observed with 2−3 V bias. Each hollow circle represents one data point, while each solid circle represents two overlapping data points.

A typical series of KPFM imaging and manipulation results are shown in Figure 2. The topographic image in Figure 2A, obtained simultaneously with the CPD image in Figure 2B, shows two Au NPs separated by ∼100 nm. Charge state manipulation was performed on the 7 nm high NP on the right in the figure, while the untouched NP on the left served as a control. Throughout the whole imaging and manipulation process the topography of the two NPs (height and separation) remained unchanged. We find that while the CPD of the right NP was modified following the process described in Figure 1, the CPD of the left particle remained constant throughout the whole charging and discharging process. After a tip−NP contact with −1 V sample bias, the CPD of the right NP increased by ∼50 mV (from −180 to −130 mV) (Figure 2B,C). This modified charge state remained stable until we contacted the NP again using the tip with V_s = 0 V (while the tip was grounded). After this zero bias contact, we found that the CPD of the NP was reset to the original value (−180 mV) (Figure 2D), indicating that the charge state of the system was restored. After another tip−NP contact with V_s = 1 V, the CPD of the NP decreased by ∼80 mV (reaching −260 mV) (Figure 2E). After a voltage pulse of V_s = −1 V, the system was reset to its original charge state (Figure 2F). Note that we found that a voltage of V_s = 0 V did not modify the CPD. The difference in the required discharge voltage for the positive versus negative charged systems is likely due to the asymmetry in the energy landscape of the metastable molecular configurations (NH_2 and NH_3 states), as discussed later.

Following the same procedure, we performed charging and discharging experiments on a series of Au NPs within the size range 7−9 nm. We were able to alter the charge state of the NP in both directions, up or down, with voltages in the +3 to −3 V range. Figure 3A summarizes the results on the CPD change after tip contact at different bias. In agreement with the results shown in Figure 2, positive bias always results in a decrease of CPD, while negative bias leads to an increase of CPD. The other prominent feature in Figure 3A is that the CPD change is overall larger after the application of a larger bias, revealing the presence of a series of stable charge states. An important observation is that the CPD of the charged Au NP/GOM system remained stable for at least 10 h in an inert nitrogen atmosphere (in an environmental chamber of the AFM) at room temperature (Figure S1, Supporting Information).

We further measured NPs of other sizes and found similar charging and discharging behavior for all the NPs with a diameter between 2.5 and 20 nm. Figure S2 shows the charge manipulation results of a 2.5 nm NP.

According to our previous results and calculations,[17] without tip contact, only one stable charge state exists in electrostatic equilibrium for a given NP size. Therefore, the existence of multiple stable states induced by tip contact could be due to either defects or redox charging in the Si substrate or structural reorganization of the GOM. Although the Si surface could have trace amounts of defects, no surface defect-induced charge memory has ever been reported in Si during the past few decades of research. We thus conclude that the GOM is responsible for the observed memory effect.

Previous work has shown that some molecules with nitro and/or amino groups exhibit conductance switching behaviors[6−9] and propose that conformational changes in the molecules could be responsible for such effects. However, to our knowledge there is no published experimental evidence or theoretical calculation to confirm the coupling of molecular conformation to the electrical conductance. To examine whether the amine groups in our GOM are responsible for the observed charge memory effects, we performed the same charging procedures on control samples where the GOM is replaced by a nonaminated molecule $-(CH_2)_6-COO-$ (inset of Figure 3B). We found that no CPD change occurred in the Au NP/nonaminated GOM except at high positive bias (≥2 V) (Figure 3B). However, the CPD change at this high bias is small and irreversible, indicating that it is likely due to permanent damage to the molecules. Therefore, we conclude that the amine group in the GOM is indeed an essential factor contributing to the charge state memory effects in the Au NP−GOM−Si system. As we explain in the following, the existence of multiple charge states of a Au NP can be explained by the bistable molecular configurations of the series of aminated molecules in contact with the NP.

To understand how the charge memory effects observed with the aminated GOM molecules could be related to configuration changes of the molecules, we performed density functional theory (DFT) calculations to determine the energy of the Au NP−aminated molecule system as it adopts different conformations. In the simulation, the $(-(CH_2)_6-CO-NH-(CH_2)_2-NH_2)$ molecule is initially connected to Au through the amino (NH_2) group (Figure 4A). The Si substrate on the other side of the GOM is not included. After structural relaxation we found two possible distortions leading to final

DOI: 10.1021/acsanm.9b01182
ACS Appl. Nano Mater. XXXX, XXX, XXX−XXX

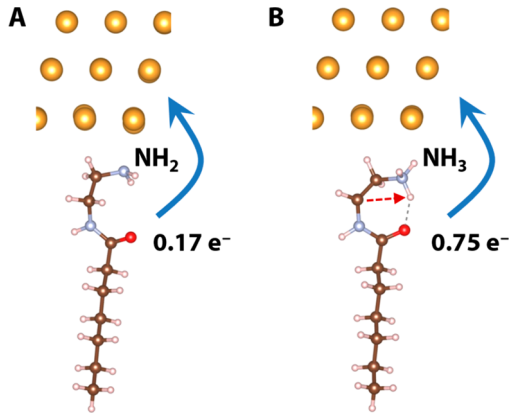

Figure 4. Bistability of the molecular configuration. (A) Stable, minimum energy configuration where the terminal NH_2 group hybridizes with Au; the resulting amount of Bader charge transfer is 0.17 e^-. (B) Possible metastable configuration as a result of proton transfer. A distortion of the molecular end group leads to a proton transfer from a CH_2 group to the terminating NH_2 group, resulting in the formation of NH_3. In this case the Bader charge transfer to Au is 0.75 e^-. This configuration is another minimum energy state relative to small distortions.

configurations that result in charge retention. We describe here the one that appears more stable. For completeness another is described in the Supporting Information. In both models the reference structure has the alkyl chain straight, with its terminal NH_2 in the chain end ($-CO-NH-(CH_2)_2-NH_2$) binding to Au through the N atom (Figure S4). This binding is the well-known dative bond where the amine group donates its lone pair to form a coordinate covalent Au−N bond.[27] The description agrees with a Bader analysis[28] that shows a net charge transfer (0.17 e^-) from the molecule to coordinately unsaturated surface Au atoms. There is another *local* minimum energy configuration, shown schematically in Figure 4B, where the molecule terminates with an NH_3, the H coming from the second CH_2 group, and forming a H-bond with the O in the carboxyl group. This configuration bears a positive excess charge, with the Bader analysis indicating a charge transfer to Au of 0.75 e^-.

One can go from the NH_2 to the NH_3 terminated configurations by distortions of the $—CO—NH—(CH_2)_2—NH_2$ group involving rotations around N—C and C—C bonds which bring the NH_2 group close to the C═O group. The energy of several intermediate configurations is shown in Figure 5A, with schematics of these configurations (labeled a–e) shown in Figure 5C. We found that all the configurations away from the initial NH_2 have higher energy, including the local energy minimum of the final NH_3 configuration, which is 0.97 eV higher than that of the initial NH_2 ground state. The energy of the configurations from the initial NH_2 to the final NH_3 goes through a maximum, which exhibits a barrier of 2.2 eV higher that the NH_2 configuration (1.23 eV higher than the NH_3 configuration).

In the presence of an electric field, either due to the initial charge transfer in the molecular junction or by the application of an electric bias, the energy landscape of the molecular conformation is altered. We found that an electric field of 2.7 V/nm (positive value denotes downward direction) is able to pull the energy of the NH_3 configuration to a level lower than that of the NH_2 configuration (Figure 5B). In this case the activation energy for the transition from NH_2 to NH_3 configurations is lowered to 1.67 eV. We further calculated the energy difference between the two minimum energy states in the presence of different electric field intensity, with the results shown in Figure 6A. We observe a critical field value of ~2.5 V/nm, where the energies of the NH_2 and NH_3

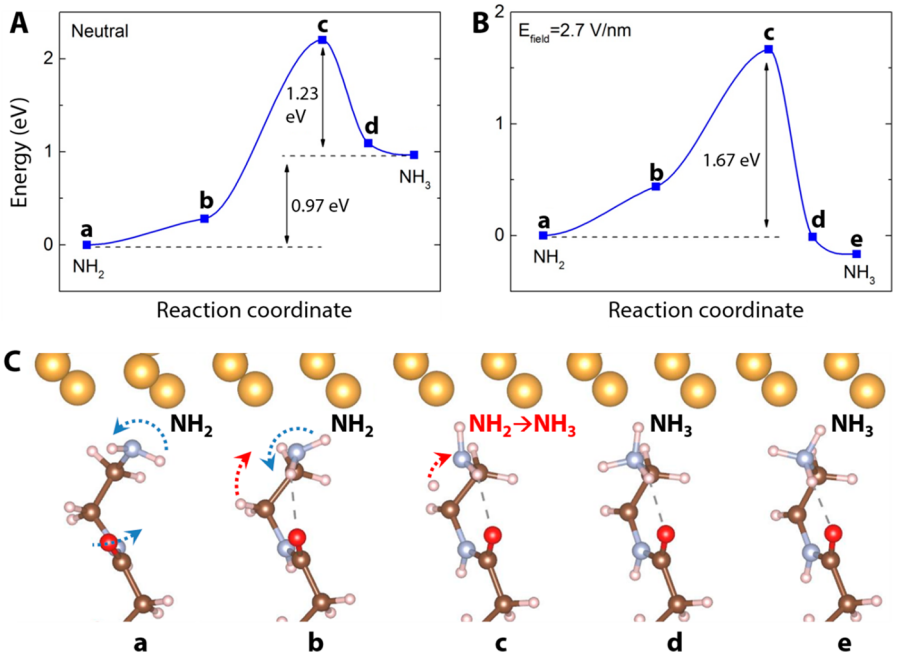

Figure 5. Energy landscape of various molecular configurations. (A) Series of possible molecular configurations in the absence of an external electric field. An energy barrier separates two minimum energy configurations, and the NH_2 termination is the most stable state. (B) Energy landscape in the presence of a positive 2.7 V/nm electric field (pointing downward). In this case the NH_3 termination is the most stable. (C) Schematic structures of the intermediate configurations (from a to e) corresponding to the states labeled in parts A and B.

DOI: 10.1021/acsanm.9b01182
ACS Appl. Nano Mater. XXXX, XXX, XXX−XXX

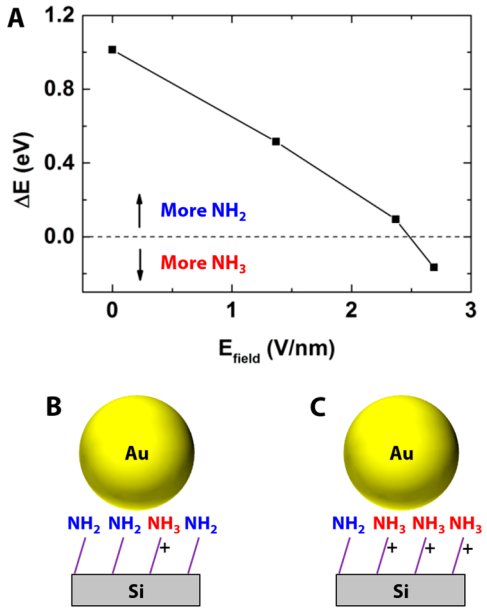

Figure 6. Multicharge stability of the Au NP−organic monolayer system. (A) Energy difference between the NH_2 and NH_3 terminated configurations as a function of applied electric field (pointing downward). (B) Schematic showing that there are more NH_2 groups (neutral) than NH_3 groups (positively charged) underneath the Au NP, in the presence of a zero or small electric field (<2.5 V/nm). (C) Schematic showing more NH_3 groups than NH_2 groups, in the presence of a large electric field (>2.5 V/nm).

configurations become equal. The higher stability of the NH_3 configuration at larger electric fields can be understood by the shift of the Au Fermi level to a position lower than the HOMO level of the $-CO-NH-(CH_2)_2-NH_2$ group (Figure S3), which leads to electron transfer from the molecule to the Au. We further found that the wave function of this HOMO level has substantial amplitude around the C−H bonds of the second CH_2 group (Figure S4). Therefore, the loss of an electron from the p_z orbital of the CH_2 group (by transfer to Au) can lead to the conversion of CH_2 to CH (namely sp^3 to sp^2) and the transfer of the H^+ to the terminal NH_2 to become NH_3^+.

In addition to modifying the energy levels of the molecular configurations, the electric field across the molecular junction also leads to electron tunneling.[17,21] These tunneling electrons can excite molecular vibrations (which may involve C−C, C−H, C−N, etc.) that further facilitate the molecular transition from the NH_2 to NH_3 state.[29,30] Note that the bending and stretching modes of the molecular bonds have energies below 0.5 eV, which can be easily excited by the tunneling electrons.

Given that most of the Au NPs have a diameter around 8 nm, we estimate that there are approximately 30 molecules in contact with each NP. Although the configuration with NH_2 termination discussed above is the most stable except at high positive fields (Figure 6A), we expect that there will always be a non-negligible number of NH_3 terminated molecules under the NP. The local electric field modifies the energy landscape of the molecular conformations (Figures 5 and 6A), while the tunneling current further excites molecular vibrations that catalyze the transformation between the NH_2 and NH_3 states. As a result, the portion of molecules in different configurations will change (Figure 6B,C). This induces a modification of the charge state of the Au NP, which depends on the ensemble of molecules and their charge configuration. When the bias is switched off, there is a large (>1 eV) barrier between the NH_2 and NH_3 configurations of each molecule, which, in the absence of tunnel current, prevents charge state switching at room temperature.

To quantify the effect of molecular switching on the potential change of the NP, we performed electrostatic simulations by treating each molecule as a point charge. As shown in Figure S6, when a molecule switches its charge state from 0 to 1, the change of potential a few nm above the NP surface will be 5−10 mV. We can thus estimate that charge state switching of ∼30 molecules underneath one NP will induce a few hundred millivolt change in the CPD of the NP. The switching of a fraction of these ∼30 molecules will lead to smaller CPD changes of the NP. This is consistent with our experimental results shown in Figure 3A.

Our combined experimental and computational results not only provide mechanistic insights into the polaron-induced molecular charge retention effects but also can enable a variety of device applications such as flexible electronics, nonvolatile memory, and neuromorphic computing.

■ ASSOCIATED CONTENT

Supporting Information

The Supporting Information is available free of charge on the ACS Publications website at DOI: 10.1021/acsanm.9b01182.

Materials and methods, charge retention test, charge manipulation of NPs with different sizes, DFT calculations, DOS of the NH_2 and NH_3 configurations under different electric field, alternative polaronic distortion model, and electrostatic simulations (PDF)

■ AUTHOR INFORMATION

Corresponding Authors

*E-mail: yjz@illinois.edu.
*E-mail: olivier.pluchery@insp.jussieu.fr.
*E-mail: mbsalmeron@lbl.gov.

ORCID

Yingjie Zhang: 0000-0002-2704-8894
Yves J. Chabal: 0000-0002-6435-0347
Javier Fernandez Sanz: 0000-0003-2064-7007
Miquel Salmeron: 0000-0002-2887-8128

Notes

The authors declare no competing financial interest.

■ ACKNOWLEDGMENTS

The work was supported by the Organic−Inorganic Nanocomposites KC3104 program, Office of Science, the Office of Basic Energy Sciences (BES), Materials Sciences and Engineering (MSE) Division of the U.S. Department of Energy (DOE) under Contract DE-AC02-05CH11231 (Y.Z., J.K., L.-W.W., M.S.). It used resources of the Molecular Foundry, supported by the Office of Science of the U.S. Department of Energy. Y.Z. acknowledges support by the University of Illinois. Y.J.C. acknowledges support by NSF Grant CHE-1300180, University of Texas at Dallas. O.P. acknowledges support by Marie Curie FP7 ILSES project (ID 612620). L.C. acknowledges support from Nanotwinning FP7 grant, NN294952, and from a Chateaubriand fellowship. J.F.S. thanks the University of Seville for support during his stage at the LBNL. We acknowledge the computational resources of the National

DOI: 10.1021/acsanm.9b01182
ACS Appl. Nano Mater. XXXX, XXX, XXX−XXX

Energy Research Scientific Computing Center (NERSC), supported by the Office of Science of the U.S. Department of Energy.

REFERENCES

(1) Lee, H.; Kim, E.; Lee, Y.; Kim, H.; Lee, J.; Kim, M.; Yoo, H.-J.; Yoo, S.; et al. *Sci. Adv.* **2018**, *4*, No. eaas9530.
(2) Oh, J. Y.; Rondeau-Gagné, S.; Chiu, Y.-C.; Chortos, A.; Lissel, F.; Wang, G.-J. N.; Schroeder, B. C.; Kurosawa, T.; Lopez, J.; Katsumata, T.; Xu, J.; Zhu, C.; Gu, X.; Bae, W.-G.; Kim, Y.; Jin, L.; Chung, J. W.; Tok, J. B.-H.; Bao, Z. Intrinsically Stretchable and Healable Semiconducting Polymer for Organic Transistors. *Nature* **2016**, *539*, 411−415.
(3) You, J.; Dou, L.; Yoshimura, K.; Kato, T.; Ohya, K.; Moriarty, T.; Emery, K.; Chen, C.-C.; Gao, J.; Li, G.; Yang, Y. A Polymer Tandem Solar Cell with 10.6% Power Conversion Efficiency. *Nat. Commun.* **2013**, *4*, 1446.
(4) Kim, E. H.; Cho, S. H.; Lee, J. H.; Jeong, B.; Kim, R. H.; Yu, S.; Lee, T.-W.; Shim, W.; Park, C. Organic Light Emitting Board for Dynamic Interactive Display. *Nat. Commun.* **2017**, *8*, 14964.
(5) Ren, J.; Vukmirovic, N.; Wang, L.-W. Nonadiabatic Molecular Dynamics Simulation for Carrier Transport in a Pentathiophene Butyric Acid Monolayer. *Phys. Rev. B: Condens. Matter Mater. Phys.* **2013**, *87*, 205117.
(6) Xin, N.; Wang, J.; Jia, C.; Liu, Z.; Zhang, X.; Yu, C.; Li, M.; Wang, S.; Gong, Y.; Sun, H.; Zhang, G.; Liu, Z.; Zhang, G.; Liao, J.; Zhang, D.; Guo, X. Stereoelectronic Effect-Induced Conductance Switching in Aromatic Chain Single-Molecule Junctions. *Nano Lett.* **2017**, *17*, 856−861.
(7) Blum, A. S.; Kushmerick, J. G.; Long, D. P.; Patterson, C. H.; Yang, J. C.; Henderson, J. C.; Yao, Y.; Tour, J. M.; Shashidhar, R.; Ratna, B. R. Molecularly Inherent Voltage-Controlled Conductance Wwitching. *Nat. Mater.* **2005**, *4*, 167−172.
(8) Chen, J.; Reed, M. A.; Rawlett, A. M.; Tour, J. M. Large On-Off Ratios and Negative Differential Resistance in a Molecular Electronic Device. *Science* **1999**, *286*, 1550−1552.
(9) Lörtscher, E.; Ciszek, J. W.; Tour, J. M.; Riel, H. Reversible and Controllable Switching of a Single-Molecule Junction. *Small* **2006**, *2*, 973−977.
(10) Schwarz, F.; Kastlunger, G.; Lissel, F.; Egler-Lucas, C.; Semenov, S. N.; Venkatesan, K.; Berke, H.; Stadler, R.; Loertscher, E. Field-Induced Conductance Switching by Charge-State Alternation in Organometallic Single-Molecule Junctions. *Nat. Nanotechnol.* **2016**, *11*, 170−176.
(11) Zhang, J. L.; Zhong, J. Q.; Lin, J. D.; Hu, W. P.; Wu, K.; Xu, G. Q.; Wee, A. T. S.; Chen, W. Towards Single Molecule Switches. *Chem. Soc. Rev.* **2015**, *44*, 2998−3022.
(12) Bi, H.; Palma, C.-A.; Gong, Y.; Hasch, P.; Elbing, M.; Mayor, M.; Reichert, J.; Barth, J. V. Voltage-Driven Conformational Switching with Distinct Raman Signature in a Single-Molecule Junction. *J. Am. Chem. Soc.* **2018**, *140*, 4835−4840.
(13) Simão, C.; Mas-Torrent, M.; Crivillers, N.; Lloveras, V.; Artés, J. M.; Gorostiza, P.; Veciana, J.; Rovira, C. A Robust Molecular Platform for Non-Volatile Memory Devices with Optical and Magnetic Responses. *Nat. Chem.* **2011**, *3*, 359−364.
(14) van de Burgt, Y.; Lubberman, E.; Fuller, E. J.; Keene, S. T.; Faria, G. C.; Agarwal, S.; Marinella, M. J.; Talin, A. A.; Salleo, A. A Non-Volatile Organic Electrochemical Device as a Low-Voltage Artificial Synapse for Neuromorphic Computing. *Nat. Mater.* **2017**, *16*, 414−418.
(15) Yang, K.; Huang, X.; He, J.; Jiang, P. Strawberry-Like Core−Shell Ag@Polydopamine@$BaTiO_3$ Hybrid Nanoparticles for High-k Polymer Nanocomposites with High Energy Density and Low Dielectric Loss. *Adv. Mater. Interfaces* **2015**, *2*, 1500361.
(16) Puebla-Hellmann, G.; Venkatesan, K.; Mayor, M.; Lörtscher, E. Metallic Nanoparticle Contacts for High-Yield, Ambient-Stable Molecular-Monolayer Devices. *Nature* **2018**, *559*, 232−235.
(17) Zhang, Y.; Pluchery, O.; Caillard, L.; Lamic-Humblot, A.-F.; Casale, S.; Chabal, Y. J.; Salmeron, M. Sensing the Charge State of Single Gold Nanoparticles via Work Function Measurements. *Nano Lett.* **2015**, *15*, 51−55.
(18) Zhang, Y.; Ziegler, D.; Salmeron, M. Charge Trapping States at the SiO_2-Oligothiophene Monolayer Interface in Field Effect Transistors Studied by Kelvin Probe Force Microscopy. *ACS Nano* **2013**, *7*, 8258−8265.
(19) Zhang, Y.; Zherebetskyy, D.; Bronstein, N. D.; Barja, S.; Lichtenstein, L.; Schuppisser, D.; Wang, L.-W.; Alivisatos, A. P.; Salmeron, M. Charge Percolation Pathways Guided by Defects in Quantum Dot Solids. *Nano Lett.* **2015**, *15*, 3249−3253.
(20) Aureau, D.; Varin, Y.; Roodenko, K.; Seitz, O.; Pluchery, O.; Chabal, Y. J. Controlled Deposition of Gold Nanoparticles on Well-Defined Organic Monolayer Grafted on Silicon. *J. Phys. Chem. C* **2010**, *114*, 14180−14186.
(21) Pluchery, O.; Zhang, Y.; Benbalagh, R.; Caillard, L.; Gallet, J. J.; Bournel, F.; Lamic-Humblot, A. F.; Salmeron, M.; Chabal, Y. J.; Rochet, F. Static and Dynamic Electronic Characterization of Organic Monolayers Grafted on a Silicon Surface. *Phys. Chem. Chem. Phys.* **2016**, *18*, 3675−3684.
(22) Zhang, Y.; Chen, Q.; Alivisatos, A. P.; Salmeron, M. Dynamic Charge Carrier Trapping in Quantum Dot Field Effect Transistors. *Nano Lett.* **2015**, *15*, 4657−4663.
(23) Zhang, Y.; Zherebetskyy, D.; Bronstein, N. D.; Barja, S.; Lichtenstein, L.; Alivisatos, A. P.; Wang, L.-W.; Salmeron, M. Molecular Oxygen Induced In-Gap States in PbS Quantum Dots. *ACS Nano* **2015**, *9*, 10445−10452.
(24) Borys, N. J.; Barnard, E. S.; Gao, S.; Yao, K.; Bao, W.; Buyanin, A.; Zhang, Y.; Tongay, S.; Ko, C.; Suh, J.; Weber-Bargioni, A.; Wu, J.; Yang, L.; Schuck, P. J. Anomalous Above-Gap Photoexcitations and Optical Signatures of Localized Charge Puddles in Monolayer Molybdenum Disulfide. *ACS Nano* **2017**, *11*, 2115−2123.
(25) Muñoz Rojo, M.; Zhang, Y.; Manzano, C. V.; Alvaro, R.; Gooth, J.; Salmeron, M.; Martin-Gonzalez, M. Spatial Potential Ripples of Azimuthal Surface Modes in Topological Insulator Bi_2Te_3 nanowires. *Sci. Rep.* **2016**, *6*, 19014.
(26) Zhang, Y.; Hellebusch, D. J.; Bronstein, N. D.; Ko, C.; Ogletree, D. F.; Salmeron, M.; Alivisatos, A. P. Ultrasensitive Photodetectors Exploiting Electrostatic Trapping and Percolation Transport. *Nat. Commun.* **2016**, *7*, 11924.
(27) Quek, S. Y.; Venkataraman, L.; Choi, H. J.; Louie, S. G.; Hybertsen, M. S.; Neaton, J. B. Amine-Gold Linked Single-Molecule Circuits: Experiment and Theory. *Nano Lett.* **2007**, *7*, 3477−3482.
(28) Henkelman, G.; Arnaldsson, A.; Jónsson, H. A Fast and Robust Algorithm for Bader Decomposition of Charge Density. *Comput. Mater. Sci.* **2006**, *36*, 354−360.
(29) Stipe, B. C.; Rezaei, M. A.; Ho, W. Coupling of Vibrational Excitation to the Rotational Motion of a Single Adsorbed Molecule. *Phys. Rev. Lett.* **1998**, *81*, 1263.
(30) Mugarza, A.; Shimizu, T. K.; Ogletree, D. F.; Salmeron, M. Chemical Reactions of Water Molecules on Ru(0001) Induced by Selective Excitation of Vibrational Modes. *Surf. Sci.* **2009**, *603*, 2030−2036.

DOI: 10.1021/acsanm.9b01182
ACS Appl. Nano Mater. XXXX, XXX, XXX−XXX